Estimation of grassland nitrogen content using UAV ultra-wide RGB images

Rebeca C. E. da Silva [1], Antonio M. G. Tommaselli [1], Nilton N. Imai [1], Rorai P. Martins-Neto[2], Daniel S. da Silveira[3], Edemar Moro[3]

[1] Department of Cartography, São Paulo State University (UNESP) at Presidente Prudente, São Paulo, Brazil – (rebeca.campos, a.tommaselli, nilton.imai)@unesp.br
[2] Faculty of Forestry and Wood Sciences, Czech University of Life Sciences Prague, Kamycka 129, 16500 Prague, Czech Republic – pereira_martins_neto@fld.czu.cz
[3] University of Western São Paulo (UNOESTE) at Presidente Prudente, São Paulo, Brazil – dsilveira33@yahoo.com.br and edemar@unoeste.br

Keywords: nitrogen content, grassland, machine learning, ultra-wide images, UAV, remote sensing.

Abstract

Nitrogen content is essential for grass growth, grassland management and forage productivity. In general, the nitrogen amount is indirectly estimated using manual techniques for sample acquisition and laboratory analysis, which are a costly endeavour, mainly in large agricultural areas. In this context, remote sensing technologies allow monitoring important parameters for agriculture, fast, non-destructively and on a large scale, using aerial images obtained by Unmanned Aerial Vehicles (UAV) and analysed through spectral indices and structural variables of the vegetation. However, further studies are needed that use more affordable sensor systems that can be used in large areas, such as in Brazil. This work assesses the feasibility of employing GoPro wide-angle RGB camera onboard a UAV to estimate the nitrogen content of an experimental grassland area. Different data scenarios were evaluated, incorporating combinations of vegetation indices (VIs) and three-dimensional (3D) metrics derived from the Canopy Height Model (CHM): all available metrics (ALL), a subset of three VIs combined with four 3D metrics (VI_3 + CHM_4), and 3D metrics only. To estimate nitrogen content, the Random Forest (RF) machine learning algorithm was applied. The most accurate model, yielding the lowest error, resulted from integrating data from two acquisition dates, achieving a coefficient of determination (R^2) of 0.83 for the model, a Pearson Correlation Coefficient (PCC) of 0.82 in the validation trials, and a Root Mean Square Error expressed as a percentage (RMSE%) of 19.62%. These findings highlight the potential of UAV-mounted RGB sensors as an effective tool for estimating pasture parameters.

1. Introduction

Brazil is among the leading countries in grassland land use, which occupies approximately 154 million hectares (Mapbiomas, 2021). The monitoring of these pasture areas conducted by Mapbiomas (2021) revealed that 38% showed intermediate degradation and 14.3% showed severe degradation. From the perspective of national agriculture, pasture degradation is one of the biggest challenges for producers. This is due to the increase in the stocking rate, the loss of nutrients due to inadequate pasture management, followed by a lack of correction and fertilisation in the formation of the grass (Zimmer et al., 2012). Among the factors contributing to this degradation is nutritional deficiency, mainly in nitrogen (Zimmer et al., 2012).

Nitrogen (N) is an essential macronutrient for plant development, as it is directly related to the synthesis of proteins, enzymes and chlorophyll (Gomide; Paciullo; Martins, 2020). Along with estimating the dry mass of the grass, estimating nitrogen in the grassland is fundamental for its management and fertilisation, avoiding both nutritional deficiencies and excesses that can cause environmental damage (Gomide; Paciullo; Martins, 2020; Lussem et al., 2022; Oliveira et al., 2023). Traditionally, N estimation has been carried out indirectly using destructive techniques for sample collection and laboratory analysis, methods which, although effective, are expensive, time-consuming and not very viable on a large scale.

In this scenario, approaches based on remote sensing and photogrammetry technologies and techniques make it possible to optimise the monitoring of pasture parameters by using optical sensors embedded in Unmanned Aerial Vehicles (UAV) (Näsi et al., 2018; Lussem et al., 2022; Oliveira et al., 2023). Off-the-shelf RGB cameras, such as the GoPro Hero4 (GoPro, 2024), offer a reduced cost and access to high spatial resolution images, despite having a lower radiometric resolution when compared to multispectral cameras. Although wide-angle cameras have disadvantages associated with distortion at the edges of the image, they can generate consistent photogrammetric products when processed with appropriate calibration models, such as those available in the photogrammetric software Metashape (Agisoft LLC, 2022). Furthermore, the wide field of view facilitates image triangulation by increasing the number of intersections, which makes the adjustment more stable. Thus, in surveys of greater spatial extent, this type of camera can be used as a viable alternative.

The photogrammetric processing of images enables the spectral behaviour of vegetation to be assessed when different normalised spectral indices are applied, as well as the creation of digital models to extract spatial characteristics of the plant, such as the Canopy Height Model (CHM). When this information is used as input data in Machine Learning (ML) models, such as Random Forest, it is possible to improve the accuracy of grassland parameter estimates. Oliveira et al. (2023) demonstrated that the integration of spectral and structural features is a cost-effective and robust approach to monitoring grassland parameters.

Due to the huge extent of pasture areas in Brazil and the importance of proper management, it is necessary to carry out studies that analyse nitrogen estimation using non-destructive and efficient techniques. Therefore, the aim of this study is to

This contribution has been peer-reviewed. The double-blind peer-review was conducted on the basis of the full paper.
https://doi.org/10.5194/isprs-annals-X-3-W4-2025-99-2026

investigate the feasibility of estimating the concentration of nitrogen in the grassland using spectral and structural information extracted from images acquired by the GoPro Hero4 ultrawide camera coupled to a UAV, contributing to research into sustainable grazing management. This work is a continuation of the study published by Da Silva et al. (2024), in which dry mass estimation techniques were applied to images captured with a GoPro camera. In this study, the same methodological approaches were applied to estimate the concentration of nitrogen in the grass.

2. Study area and data acquisition

The study site is located on an experimental farm in the Nova Pátria district, within the municipality of Presidente Bernardes, São Paulo state, Brazil (22°17'4.85"S, 51°40'46.31"W) (Figure 1), owned by UNOESTE University. RGB imagery was captured using a GoPro Hero4 Black action camera equipped with a super wide-angle lens (Table 1), mounted on a UX4 quadcopter UAV. The initial flight campaign (18/01/2021) comprises 155 images, while the subsequent flight campaign (27/03/2021) comprises 147 images, with a flight height of 80 m above ground in both cases. Ground Control Points (GCPs) were surveyed using GNSS receivers for the bundle block adjustment (8 GCPs). Since the terrain is dirty and covered with grass, some GCPs were signalised with concrete plates, while others were marked directly on the ground with lime powder, in the form of a circle with a diameter of approximately 0.20 m.

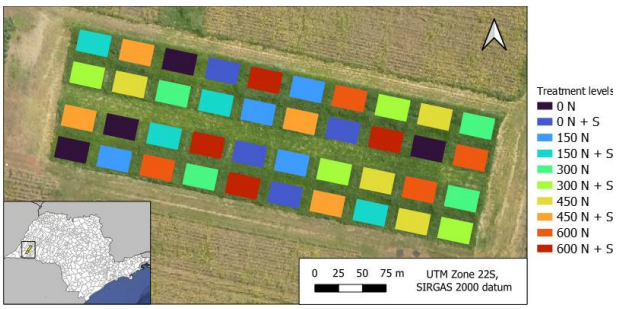

Figure 1. Location of Brachiaria grass plots at the Unoeste Experimental Farm, Presidente Bernardes, São Paulo, Brazil.

Details	Specifications
Camera model	GoPro HERO4 Black
Focal length	3 mm
Pixel size	1.73 × 1.73 µm
Image size	4000 × 3000 pixels (12 MP)
Sensor size	6.17 × 4.55mm CMOS (1/2.3")
Dimensions	41 mm × 59 mm × 30 mm
Camera weight	152 g
Output format	JPEG

Table 1. Camera specifications.

A total of 40 grass plots, measuring 3.5 × 5.0 m each, comprising the species *Urochloa Brizantha*, also known as *Brachiaria brizantha*, were used in the experiment. Each plot had four repeats of chemical treatment following a randomised block design in a 5 × 5 factorial scheme, considering 10 combinations of five levels of nitrogen (N) (0, 150, 300, 450, 600 kg/ha) and five levels of sulphur (S) (0, 150, 300, 450, 600 kg/ha). The field reference sample was acquired employing a metal rectangle (measuring 0.25 × 0.25 m), to cut an area of 0.5 m² of grass per plot. Sampling was carried out randomly by placing a standard frame over areas with higher grass density, following a procedure similar to the "quadrats" method (Salman, 2006). Fresh and dried grass were weighed to determine the dry matter (DM). The samples were collected on both dates and set aside for laboratory analysis. Sequentially, nitrogen content in kg/ha was determined using the micro Kjeldahl method (AOAC, 1984), dividing the crude protein by the factor 6.25, then multiplying the result by the DM value of each plot. The mean weight and standard deviation of the nitrogen content in grass samples are shown in Table 2.

Sampling date	Mean (kg/ha)	Std (kg/ha)
11/01/2021	DM: 2601.35	DM: 513.21
	N: 41.77	N: 8.80
29/03/2021	DM: 4740.53	DM: 1276.07
	N: 94.64	N: 34.79

Table 2. Dry mass (DM) and nitrogen content (N): Mean and standard deviation (SD) of first and second cut data.

3. Methodology

3.1 Geometric processing

The aerial images collected during the flight campaigns were processed with the Agisoft Metashape software, version 1.8.4 (Agisoft LLC, 2022). In general, this software uses Structure from Motion (SfM) to generate the initial reconstruction and Bundle Adjustment to refine and improve interior and exterior orientation parameters, as well as to generate a three-dimensional digital terrain model.

Image processing was performed using Metashape, employing the fisheye camera model, as recommended for this type of sensor. Six ground control points (GCPs) and two check points (CPs) were employed for georeferencing through in-situ calibration. Detailed processing specifications are provided in Da Silva et al. (2024). Image processing followed the general phototriangulation workflow: the images were initially aligned (*medium*–quality setting), generating a sparse point cloud, and the GCPs were identified in the images. In a second alignment (*high*–quality setting), the point cloud was manually and automatically filtered to remove points with gross errors (outliers). Subsequently, the three-dimensional digital surface model was refined with the parameters estimated during the model's georeferencing process (*optimize camera alignment*) to compute a *high*–quality dense point cloud (Figure 2.a) with *mild* depth filtering, using the final estimated values for the exterior and interior orientation parameters, completing the bundle adjustment stage.

The Digital Surface Models (DSM) were generated from the dense point cloud, and the Digital Terrain Model (DTM) was generated from the classification of the point cloud, both exported with a Ground Sample Distance (GSD) of 10 cm. The orthomosaic was exported with a GSD of 5 cm. The Canopy Height Models (CHM) were computed using the difference between the MDS and MDT in the QGIS software, version 3.34.35 (QGIS Development Team, 2023). The quality of the results was checked by observing whether the Root Mean Square Error (RMSE) of the GCPs was smaller than the GSD value of the products.

3.2 RGB vegetation indexes and 3D metrics

The vegetation indices, derived from the RGB channels, employed in this study, were calculated using the raster calculator in QGIS and included only normalised spectral indices. It is

important to note that the GoPro camera does not provide the spectral bandwidth information for each RGB channel, which limits the spectral precision of the indices. As a result, only normalised RGB-based indices were adopted in this work: Red Green Blue Vegetation Index Excess (RGBVI), Green Leaf Index (GLI), Grassland Index (GrassI), Normalised Green Red Difference Index (NGRDI) and Plant Pigment Ratio Index (PPRI). For completeness, Table 3 provides a summary of these indices along with their respective formulas and references.

Additionally, eight three-dimensional (3D) metrics were extracted from the CHMs: maximum height, minimum height, mean height, median height, standard deviation of height, and the 30th, 60th, and 90th height percentiles. These metrics were calculated using a custom script in R, version 4.3.2 (R Core Team, 2023).

Equations	Authors
$GrassI = RGBVI + CHM$	(Bareth et al., 2015)
$RGBVI = \frac{G^2 - (R * B)}{G^2 + (R * B)}$	(Bendig et al., 2015)
$GLI = \frac{2G - R - B}{2G + R + B}$	(Gobron et al., 2000)
$\mathrm{PPRI} = \frac{\mathrm{G} - \mathrm{B}}{\mathrm{G} + \mathrm{B}}$	(Metternicht, 2003)
$\mathrm{NGRDI} = \frac{\mathrm{G} - \mathrm{R}}{\mathrm{G} + \mathrm{R}}$	(Tucker, 1979)

Table 3. Vegetation Indices for RGB images.

3.3 Feature extraction process

Given the absence of accurate georeferencing of the field samples (see section 2), it was necessary to adapt the attribute extraction approach by delineating representative sampling areas based on the spatial distribution of vegetation visualised in the images of each date. To implement this approach, the QGIS software was used, following the steps described in Da Silva et al. (2024).

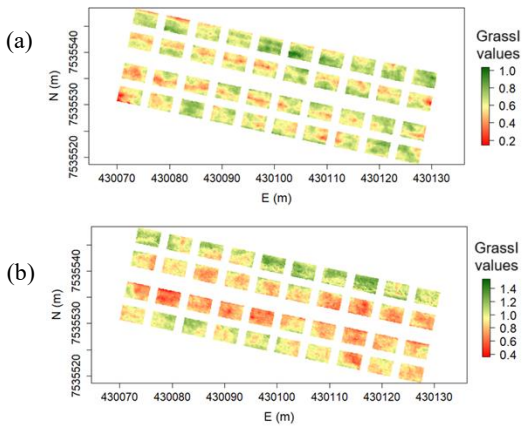

Figure 2. GrassI vegetation index image of the grass on 18 January (a) and 27 March 2021 (b).

Overall, the Grass index image (Figure 2) was categorised into eight classes at equal intervals to generate the polygons for extracting attributes for each date. The resulting classification was used to generate polygons corresponding to the different index ranges. For each plot, polygon classes with the lowest index values – corresponding to areas of low grass density – were discarded. Polygons from the classes with the highest index values were selected to represent the regions with the highest grass density, which are likely to correspond to the collected field samples. A single polygon was generated per plot (n = 40) by merging these polygons, which correspond to the regions with the highest distribution of grass. This final shape file was used as the basis for extracting the attributes, the mean values of VI images, based on RGB channels, and the 3D metrics derived from the CHM.

For each acquisition date, 13 attributes were extracted per plot: five mean vegetation index (VI) values and eight structural metrics. This means that with 40 plots, the data set per date consisted of 520 values (200 VI + 320 3D metrics). Consequently, the final dataset, which includes the two dates, contains a total of 1040 attributes (400 VI + 640 3D).

3.4 Regression model and quality assessment

The estimation process was implemented in R using the Caret (Kuhn, 2008) and Random Forest (Breiman, 2001) packages. Random Forest is a regression algorithm based on multiple decision trees generated from random subsets of the data and attributes (Breiman, 2001). The final prediction is obtained by the mean of the trees' predictions, which reduces overfitting and improves the model's generalisation.

Considering the number of field samples (n = 40), with one nitrogen value per plot, the models generated with the RF were calibrated using the repeated cross-validation technique (*repeatedcv*), with 10 iterations, each with 5 repetitions. This approach reduces overfitting and provides more robust estimates of performance, based on the mean values of the metrics obtained in the repetitions. The number of trees (*ntree*) was kept at the default value (500), and the number of variables per split (*mtry*) was defined as the square root of the number of attributes (Gislason; Benediktsson; Sveinsson, 2006). The data set was divided into 70% for training and 30% for validation. Pearson correlation and Principal Component Analysis (PCA) were applied to assess the correlation and contribution of the variables in the modelling.

Overall, nine regression models were tested in three scenarios described in Table 4: (i) use of all spectral attributes and 3D metrics; (ii) only 3D metrics; and (iii) a reduced set with 3 spectral attributes and 4 height metrics, selected by importance analysis (Pearson correlation, PCA and initial tests). The models were applied to the two flight campaigns, individually and combined, both to estimate nitrogen concentration.

Context	Models	Number of attributes
18/01	ALL	13
	CHM_{all}	8
	$VI_3 + CHM_4$	7
27/03	ALL	13
	CHM_{all}	8
	$VI_3 + CHM_4$	7
Fusion	ALL	13
	CHM_{all}	8
	$VI_3 + CHM_4$	7

Table 4. Description of the regression models fitted with different sets of variables in three contexts.

This contribution has been peer-reviewed. The double-blind peer-review was conducted on the basis of the full paper.
https://doi.org/10.5194/isprs-annals-X-3-W4-2025-99-2026 | © Author(s) 2026. CC BY 4.0 License.

The performance of the models in the training set was assessed using the coefficient of determination (R^2), root mean square error (RMSE) and percentage RMSE (RMSE%). Pearson correlation, RMSE and RMSE% were used for validation. These metrics were chosen to enable comparison with the results of similar studies published.

4. Results

4.1 Visual CHM analysis

The photogrammetric processing yielded satisfactory results, with errors within the centimetre range, as shown in Table 5. The root mean square error (RMSE) for the planimetric coordinates (X, Y) and the altimetric component (Z) remained below one ground sampling distance (GSD). Additionally, the total RMSE of the projections of the GCPs in the images was subpixel in both flight campaigns.

Date	$X_{(cm)}$	$Y_{(cm)}$	$Z_{(cm)}$	$3D_{(cm)}$	$Image_{(px)}$
01/18/2021	0,31	0,71	3,21	3,26	0,46
03/27/2021	0,31	1,79	1,85	2,25	0,54

Table 5. RMSE on the check points.

The wide field of view of the GoPro Hero 4 proved to be advantageous, since it enhanced the identification of ground control points by increasing the number of tie points shared across images with multiple intersecting rays for each point. It was observed that 270 images contained check points on date 01/18/2021 and approximately 254 images on date 03/27/2021. As a result, the reprojection error remained around 0.5 pixels.

Figure 3 illustrates the RGB mosaics and their respective CHMs per plot for the flight campaigns, with the colour corresponding to the grass height in the 0-1 m range. A heterogeneous spatial distribution of grass is visually noticeable in each plot, including those exposed to the same treatment levels. From a visual inspection of the orthomosaics, it is possible to note that within some plots, there are gaps in the grass. These flaws may be associated with heavy machinery traffic during management, as well as factors external to the experiment, such as environmental variations or specific flaws in crop establishment. In the 18 January campaign (Figure 3a), the grass was in an initial stage of growth, with a maximum height of approximately 0.6 cm for a few plots. In contrast, the height values of the 27 March campaign (Figure 3b) were significantly higher, approaching 1 m, due to the vegetation growing from one date to the next.

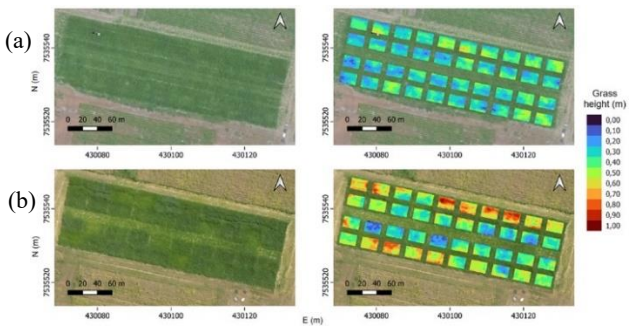

Figure 3. Orthomosaics and Canopy Height Models (CHM) of the grass on 18 January (a) and 27 March, 2021 (b).

4.2 Correlation analysis and variables contribution

The variables presented in the Pearson correlation matrix include both metrics derived from images obtained by UAV and the amount of nitrogen per plot obtained from field samples. The correlation matrix was used to verify the linear relationship between these variables, highlighting those with the greatest potential to explain dry mass variability over time. Figure 4 shows Pearson 's correlation matrix, in which the colours indicate the direction of the correlations (red for negative and blue for positive), and the size of the circles represents the intensity. The analysis shows that the GrassI index exhibits the highest correlation with nitrogen (r = 0.7), surpassing other indices, which shows correlations around r = 0.5. In contrast, the NGRDI index showed the weakest negative correlation (r = -0.5). The 3D metrics showed moderate and positive correlations (~r = 0.7), except for CHM_{std}, which had a lower correlation (r = 0.4).

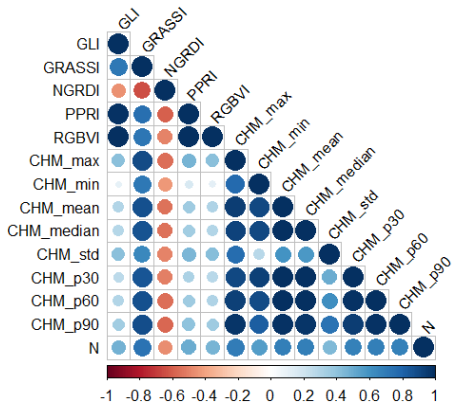

Figure 4. Pearson's matrix correlation between variables.

Based on the same data, PCA was applied to reduce the dimensionality of the variables and identify the most relevant patterns of variation. The first two components were analysed, as together they explained most of the variability in the data. In the principal component analysis, PC1 explained 68.7% of the total variance, with emphasis on the GrassI index and 3D metrics such as CHM_{p90}, CHM_{max} and CHM_{median}. PC2 explained 20.8% of the variance.

4.3 Regression model

The training (Table 5) and validation (Table 6) results for nitrogen content varied according to the input variables. Three model types were tested: using all variables (ALL), only 3D metrics (CHM_{all}), and a selected set based on correlation and empirical tests (VI_3 + CHM_4), which included the indices GrassI, PPRI, RGBVI, and the 3D metrics CHM_{min}, CHM_{mean}, CHM_{p30}, and CHM_{p60}.

For the 18 January training data set, the IV_3 + CHM_4 model obtained the lowest RMSE of 8.12 kg/ha. For the 27 March train data, the lowest RMSE of 22.87 kg/ha was obtained by the ALL set. Combining the training data from the two dates, the IV_3 + CHM_4 model was the best adjusted, with the highest R^2 of 0.83 and the lowest RMSE of 18.78 kg/ha.

Evaluating the results of the validation data for 18 January, the ALL model had the lowest percentage RMSE of 16.67%, equivalent to 6.92 kg/ha, even with a PCC of 0.51. For the 27 March models, the ALL and VI_3 + CHM_4 models achieved close results, but the VI_3 + CHM_4 model had the lowest percentage RMSE, equivalent to 23.28%. For the combined data set, the VI_3 + CHM model achieved the lowest RMSE of 12.0 kg/ha and

percentage RMSE of 19.62%. Overall, the models with the CHM_{all} variables only, had the worst RMSE values.

Date	Variable	R^2	RMSE (kg/ha)
18/01	ALL	0.56	8.61
	CHM_{all}	0.63	9.24
	$VI_3 + CHM_4$	0.51	**8.12**
27/03	ALL	0.75	**22.87**
	CHM_{all}	0.66	31.42
	$VI_3 + CHM_4$	0.75	24.64
Fusion	ALL	0.76	20.66
	CHM_{all}	0.57	25.93
	$VI_3 + CHM_4$	0.83	**18.78**

Table 5. Coefficient of determination (R^2) and RMSE for training data of nitrogen concentration (N) models.

Date	Variable	PCC	RMSE (kg/ha)	RMSE%
18/01	ALL	0.51	6.92	**16.67**
	CHM_{all}	0.41	7.64	19.47
	$VI_3 + CHM_4$	0.58	7.80	19.35
27/03	ALL	0.86	23.36	23.83
	CHM_{all}	0.58	26.31	26.39
	$VI_3 + CHM_4$	0.84	25.42	**23.28**
Fusion	ALL	0.92	16.04	23.37
	CHM	0.85	19.63	28.62
	$VI_3 + CHM_4$	0.92	12.00	**19.62**

Table 6. Pearson Correlation Coefficients (PCC), Root Mean Squared Error (RMSE) and RMSE% for validation data of nitrogen concentration (N) models.

In general, considering the order of importance of the variables for each model, the PPRI and RGBVI indices were the most important in the different models. In addition, the CHM_{p30} metric consistently remained in an intermediate position among the variables in almost all the models that estimated the amount of nitrogen in the grass. When analysing the models using the combination (Fusion) of the two dataset dates, the main attributes identified were: PPRI, RGBVI, GRASSI, CHM_{mean} and CHM_{max}.

5. Discussion

Due to the lack of information on the spectral ranges of the GoPro's RGB channels, it was not possible to apply an absolute radiometric calibration. Because of this, vegetation indices were calculated based on digital numbers (ND) and normalised differences, to reduce variations in illumination and enhance the contrast between vegetation and soil (Silleos et al., 2006; Zhang et al., 2022)).

Although most of the visible radiation (0.4-0.7 µm) is absorbed by leaf pigments such as chlorophyll (Bannari et al., 1995), a fraction is still reflected. Nitrogen is directly related to chlorophyll synthesis (Evans, 1989), so plants well supplied with N accumulate more photosynthetic pigments. This process results in visually greener leaves and, spectrally, greater absorption in the blue and red bands. For this reason, indices based on RGB bands can be applied to assess vegetation, as they capture information linked to photosynthesis, senescence and the physiological state of plants. The PPRI and RGBVI indices showed a strong relationship with chlorophyll content and, consequently, with nitrogen status.

Analysing the progression of grass growth between campaigns, it is consistent with field data that indicate a substantial increase in dry mass and nitrogen concentration from January to March. This confirms the expected biomass accumulation and nutrient uptake associated with the vegetative growth during the rainy season. Since the experiment was conducted on an experimental farm, variations in grass height on the same plot under the same chemical treatments may be a result of previous management practices that influenced soil conditions, inherent soil variability in the area, and differences in environmental factors. Under these conditions, 3D metrics allowed us to capture structural differences between plants with higher and lower biomass accumulation, which may be related to nitrogen uptake.

When comparing the results of this study with previous research that used RGB spectral indices and height metrics to estimate nitrogen concentration using the Random Forest algorithm, the works of Näsi et al. (2018), Lussem et al. (2022) and Oliveira et al. (2023) are noteworthy. Näsi et al. (2018) used a Samsung NX500 (RGB) camera to estimate the nitrogen content in Barley, based on 36 sampling areas and data collected at a flight height of 140 meters. Using only 3D metrics, they achieved a PCC of 0.87 and RMSE% of 39.6. When combining spectral data with three-dimensional metrics, the results improved significantly, with a PCC of 0.94 and RMSE% of 25.2. Lussem et al. (2022) estimated nitrogen in *Lolio-Cynosuretum* pastures, based on 156 sampled areas, using spectral and 3D attributes. The model showed an RMSE% of 24.5. When the RGB and multispectral data obtained by the MicaSense RedEdge-M and Sony Alpha 7r cameras were combined, the error was even lower, with an RMSE% of 17.9. In the study by Oliveira et al. (2023), which evaluated the nitrogen content in forage for silage (*Phleum pratense L.*) with different spectral bands, the RGB data resulted in an RMSE% of 9.04, while the 3D metrics showed one of the lowest correlation values (PCC = 0.80), even with 60 training samples. The best results were obtained with spectral attributes extracted from the AFX10 hyperspectral camera (VNIR), achieving an RMSE% of 7.44.

6. Conclusion

This study showed that it is possible to estimate nitrogen concentration from RGB images obtained with an ultra-wide action camera, GoPro Hero4. To date, no studies have been found in the literature that have used RGB action cameras to estimate nitrogen in the grassland, which highlights the innovative and affordable nature of this approach.

The combination of RGB spectral indices, based on normalised differences, with three-dimensional metrics derived from height models showed promising performance, considering the errors associated with manual sampling in the field. Considering the combination of data from the two flight campaigns, the $VI_3 + CHM_4$ model achieved RMSE of 19.62% and $R^2 = 0.92$, suggesting that spectral and structural attributes offer complementary information. The results obtained do not differ significantly from those reported in studies using multispectral sensors, which is relevant, especially given that the GoPro camera is a more affordable alternative compared to more expensive spectral sensors. Thus, the findings reinforce the potential of low-cost remote sensing, combined with machine learning algorithms, for estimating nitrogen concentration,

contributing to more efficient practices in precision agriculture. This can lead to cost savings by reducing the need for extensive field sampling.

Future studies should explore the application of transfer learning, adapting the current model to other scenarios using a reduced number of samples. Additionally, the integration of a radiance sensor to convert digital number (DN) values into reflectance could be investigated, allowing for the calculation of a broader range of spectral indices.

Acknowledgements

This study was financed in part by the Coordenação de Aperfeiçoamento de Pessoal de Nível Superior – Brasil (CAPES) (88887.961785/2024-00 and 88887.898553/2023-00), by the National Council for Scientific and Technological Development, CNPq (grants n. 130411/2022-1, 308747/2021-6 and 303670_2018-5]) and by the São Paulo Research Foundation, FAPESP (Grant: 2021/06029-7).

References

AOAC, 1984: Official methods of analysis of the Association of Official Analytical Chemists. 14th ed. Arlington, Va: AOAC.

Bannari, A., Morin, D., Bonn, F., Huete, A.R., 1995: A review of vegetation indices. *Remote Sens. Rev.*, 13(1–2), 95–120. doi.org/10.1080/02757259509532298.

Breiman, L., 2001: Machine learning. *Random Forest: Breiman and Cutler's random forests for classification and regression*, 45(1), 5–32. doi.org/10.1023/A:1010933404324.

Da Silva, R.C.E., Tommaselli, A.M.G., Imai, N.N., Martins-Neto, R.P., Da Silveira, D.D.S., Moro, E., 2024: Dry mass grassland estimation using UAV ultra-wide RGB images. *ISPRS Ann. Photogramm. Remote Sens. Spatial Inf. Sci.*, X-3–2024, 69–75. doi.org/10.5194/isprs-annals-X-3-2024-69-2024.

Evabs, J. R. Photosynthesis and nitrogen relationships in leaves of C3 plants. *Oecologia*, v. 78, n. 1, p. 9–19, 1989. https://doi.org/10.1007/BF00377192.

Gislason, P.O., Benediktsson, J.A., Sveinsson, J.R., 2006: Random forests for land cover classification. *Pattern Recogn. Lett.*, 27(4), 294–300. doi.org/10.1016/j.patrec.2005.08.011.

Gobron, N., Pinty, B., Verstraete, M.M., Widlowski, J.-L., 2000: Advanced vegetation indices optimized for up-coming sensors: Design, performance, and applications. *IEEE Trans. Geosci. Remote Sens.*, 38(6), 2489–2505. doi.org/10.1109/36.885197.

Gomide, C.A.M., Paciullo, D.S.C., Martins, C.E., 2020: Momento da adubação nitrogenada em pastagens intensivamente manejadas. Juiz de Fora, MG: Embrapa Gado de Leite.

GoPro, 2024: GoPro Hero4 Black. gopro.com/pt/br/ (19 April 2024).

Kuhn, M., 2008: Building predictive models in R using the caret package. *J. Stat. Softw.*, 28(5). doi.org/10.18637/jss.v028.i05.

Lussem, U., Bolten, A., Kleppert, I., Jasper, J., Gnyp, M.L., Schellberg, J., Bannari, A., 2022: Herbage mass, N concentration, and N uptake of temperate grasslands can adequately be estimated from UAV-based image data using machine learning. *Remote Sens.*, 14(13), 3066. doi.org/10.3390/rs14133066.

MapBiomas, 2023: Projeto MapBiomas – Mapeamento anual de cobertura e uso da terra do Brasil - coleção 6. mapbiomas-br-site.s3.amazonaws.com/Fact_Sheet_PASTAGEM_13.10.2021_ok_ALTA.pdf (28 May 2023).

Metternicht, G., 2003: Vegetation indices derived from high-resolution airborne videography for precision crop management. *Int. J. Remote Sens.*, 24(14), 2855–2877. doi.org/10.1080/01431160210163074.

Näsi, R., Viljanen, N., Kaivosoja, J., Alhonoja, K., Hakala, T., Markelin, L., Honkavaara, E., 2018: Estimating biomass and nitrogen amount of barley and grass using UAV and aircraft based spectral and photogrammetric 3D features. *Remote Sens.*, 10(7), 1082. doi.org/10.3390/rs10071082.

Oliveira, R.A., Näsi, R., Korhonen, P., Mustonen, A., Niemeläinen, O., Koivumäki, N., Hakala, T., Suomalainen, J., Kaivosoja, J., Honkavaara, E., 2023: High-precision estimation of grass quality and quantity using UAS-based VNIR and SWIR hyperspectral cameras and machine learning. *Precis. Agric.* doi.org/10.1007/s11119-023-10064-2.

QGIS Development Team. 2023. QGIS Geographic Information System. Open Source Geospatial Foundation Project. qgis.osgeo.org (1 January 2024).

R Core Team. 2023. The R Project for Statistical Computing. www.r-project.org/ (19 April 2024).

Salman, A.K.D., 2006: Método do quadrado para estimar a capacidade de suporte de pastagens. Porto Velho: Embrapa Rondônia. Disponível em: www.infoteca.cnptia.embrapa.br/bitstream/doc/710748/1/foldermetododoquadradopastagens.pdf. (9 February 2025).

Silleos, G., Alexandridis, T., Gitas, I., Perakis, K., 2006: Vegetation indices: advances made in biomass estimation and vegetation monitoring in the last 30 years. *Geocarto Int.*, 21, 21–28.

Tucker, C.J., 1979: Red and photographic infrared linear combinations for monitoring vegetation. *Remote Sens. Environ.*, 8(2), 127–150. doi.org/10.1016/0034-4257(79)90013-0.

Zhang, H., Tang, Z., Wang, B., Meng, B., Qin, Y., Sun, Y., Lv, Y., Zhang, J., Yi, S., 2022: A non-destructive method for rapid acquisition of grassland aboveground biomass for satellite ground verification using UAV RGB images. *Glob. Ecol. Conserv.*, 33, e01999. doi.org/10.1016/j.gecco.2022.e01999.

Zimmer, A.H., Macedo, M.C.M., Kichel, A.N., Almeida, R.G., 2012: Degradação, recuperação e renovação de pastagens: Gado de corte. Documentos, 189. Campo Grande, MG: Embrapa. Disponível em: www.embrapa.br/busca-de-publicacoes/-/publicacao/951322/degradacao-recuperacao-e-renovacao-de-pastagens (7 February 2024).